Fluctuations in the Aztec diamonds via a space-like maximal surface in Minkowski 3-space

Dmitry Chelkak, Sanjay Ramassamy

FLUCTUATIONS IN THE AZTEC DIAMONDS VIA A LORENTZ-MINIMAL SURFACE

DMITRY CHELKAK AND SANJAY RAMASSAMY

Abstract. We provide a new description of the scaling limit of dimer fluctuations in homogeneous Aztec diamonds via the intrinsic conformal structure of a Lorentz-minimal surface in $\mathbb{R}^{2+1}$. This surface naturally appears as the limit of the graphs of origami maps associated to symmetric t-embeddings (Coulomb gauges) of Aztec diamonds, fitting the framework of [6, 7].

1. Introduction

In this paper we discuss the homogeneous bipartite dimer model on Aztec diamonds [10]. Though this is a *free fermion* model, it is still interesting due to the presence of a *non-trivial conformal structure* generated by specific boundary conditions. We refer to a recent paper [2] and references therein for a discussion of this conformal structure from the theoretical physics perspective; see also [13] for a similar discussion in the interacting fermions context. Mathematically, this is one of the most classical and rigorously studied examples demonstrating the rich behavior of the dimer model: convergence of fluctuations to the Gaussian Free Field (GFF) in a non-trivial metric, Airy-type asymptotics near the curve separating the phases, etc. We refer the interested reader to lecture notes [12, 15] for more information on the subject.

The Aztec diamond A_n of size n is a subset $|p|+|q| \le n+1$ of the square grid $(p,q) \in (\mathbb{Z}+\frac{1}{2})^2$; see Fig. 1. The dimer model on A_n is a random choice of a perfect matching in A_n. Let

$$\diamondsuit := \{(x,y) \in \mathbb{R}^2 : |x| + |y| < 1\} \quad \text{and} \quad \mathbb{D}_\diamondsuit := \tfrac{\sqrt{2}}{2}\mathbb{D} = \{(x,y) \in \mathbb{R}^2 : x^2 + y^2 < \tfrac{1}{2}\},$$

where $\mathbb{D}$ is the unit disc. The *Arctic circle* phenomenon [14, 9] consists in the fact that the regions $\frac{1}{n}(p,q) \in \diamondsuit \setminus \overline{\mathbb{D}}_\diamondsuit$ are asymptotically frozen – the orientation of all dimers in these regions is almost deterministic – while the liquid region $\mathbb{D}_\diamondsuit$ carries long-range correlated fluctuations. A convenient way to encode these fluctuations is to consider random Thurston's height functions [19] of dimer covers. For homogeneous Aztec diamonds it is known [5, 8] that these height functions converge (in law) to the *flat* Gaussian Free Field in $\mathbb{D}$ provided that the following *change of the radial variable* $\mathbb{D}_\diamondsuit \leftrightarrow \mathbb{D}$ is made:

$$r = \sqrt{2}\rho/(1+\rho^2), \quad r = (x^2+y^2)^{1/2} \in [0, \tfrac{\sqrt{2}}{2}] \quad \leftrightarrow \quad \rho \in [0,1]. \tag{1.1}$$

In very recent developments [6, 7], the following idea arose: the conformal structure of dimer model fluctuations on abstract planar graphs can be understood via the so-called *t-embeddings* (which appeared under the name *Coulomb gauges* in the preceding work [16]; see also [1]) and the limits of the associated *origami maps*; see Section 2 for definitions. In this approach, the right parametrization of the liquid region should appear as the conformal parametrization of a certain *space-like minimal surface* embedded into the *Minkowski (or Lorentz) space* $\mathbb{R}^{2+2} \supset \mathbb{R}^{2+1}$.

We aim to test this paradigm using the classical Aztec diamonds example: in this case one should see a new interpretation of the known conformal structure described by (1.1). We give an inductive construction of relevant t-embeddings and origami maps of those, and relate them to a *discrete wave equation* in 2D. (It is worth noting that appearance of solutions of wave equations in the context of the dimer model on Aztec diamonds was observed in the foundational paper [9] already; see the discussion at the end of [9, Section 6.1].) Both analytic arguments and numerical

Date: February 18, 2020.

Key words and phrases. dimer model, Aztec diamond, Lorentz-minimal surfaces, conformal invariance.

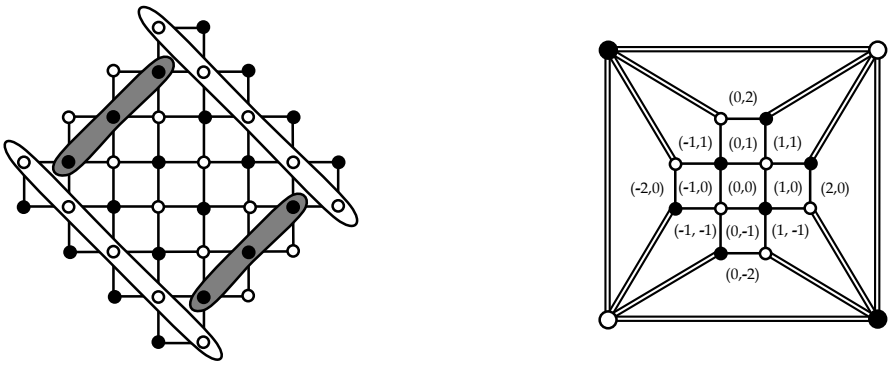

FIGURE 1. Aztec diamond A_{n+1} and its reduction A'_{n+1} for $n = 3$. Double edges of A'_{n+1} have weight 2. The labeling (j, k) of faces of A'_{n+1} is shown, $|j| + |k| < n$.

simulations strongly support the convergence of origami maps to an explicit Lorentz-minimal surface $S_\diamondsuit$ (see Fig. 5), thus confirming the relevance of the setup developed in [6, 7].

Remark 1.1. In this short note we do *not* rigorously prove the convergence of fundamental solutions of discrete wave equations to the continuous ones (see Eq. (3.4) and (3.5)) though we believe that it should not be very hard to derive. After this, the only remaining ingredient to obtain (following the general framework of [6, 7]) a new proof of the convergence of fluctuations in Aztec diamonds to the *GFF in the intrinsic metric of the surface* $S_\diamondsuit \subset \mathbb{R}^{2+1}$ would be to check a technical Assumption EXP-FAT (see [6, 7]) about faces of the t-embeddings in question. One can get some intuition on its validity from numerical simulations (e.g., see Fig. 4).

Remark 1.2. The recursive construction of the Aztec diamond via urban renewals that we use below was first introduced by Propp [17]. It provides an easy computation of the dimer partition function for the Aztec diamond with all weights equal to 1. A stochastic variant of that construction, called domino shuffling [11], samples a random dimer configuration of A_{n+1} from a random dimer configuration of A_n and additional iid Bernoulli random variables. In our analysis, the key role is played by the so-called Miquel (or central) move, which was discovered in [1, 16] to be the counterpart of the urban renewal move under the correspondence between t-embeddings and dimer models considered on abstract planar graphs. One may hope that other settings where generalizations of domino shuffling or urban renewal apply (e.g., see [3, 4, 18]) provide other explicit recursive constructions of t-embeddings. It would be interesting to further test the relevance of the framework of [6, 7] on such examples, especially in presence of gaseous bubbles which should lead to Lorentz-minimal cusps of the surface.

2. T-EMBEDDINGS AND ORIGAMI MAPS OF AZTEC DIAMONDS

2.1. **The Aztec diamond and its reduction.** Let $n \geq 1$ be a positive integer and consider the square grid $(\mathbb{Z}+\frac{1}{2})^2$ with vertices having half-integer coordinates. We define A_{n+1}, the *Aztec diamond* of size $n+1$ to be a subgraph of this square grid formed by vertices $(p, q) \in (\mathbb{Z} + \frac{1}{2})^2$ such that $|p| + |q| \leq n + 1$. Independently of the parity of n, we assume that the north-east ($p+q = n+1$) and south-west ($p+q = -n-1$) boundaries of A_{n+1} are composed of black vertices (while the north-west and south-east boundaries are composed of white ones); see Fig. 1. We consider the homogeneous dimer model on A_{n+1}, each edge has weight 1.

It is well known that correlation functions of the dimer model remain invariant under the following transforms (e.g., see [16, Fig. 1] or Fig. 2 below):

- contraction of a vertex of degree 2 (if the two edge weights are equal to each other);
- merging of parallel edges, the new edge weight is equal to the sum of initial ones;
- gauge transformations, which amount to a simultaneous multiplication of weights of all edges adjacent to a given vertex by the same factor;
- the so-called urban renewal move.

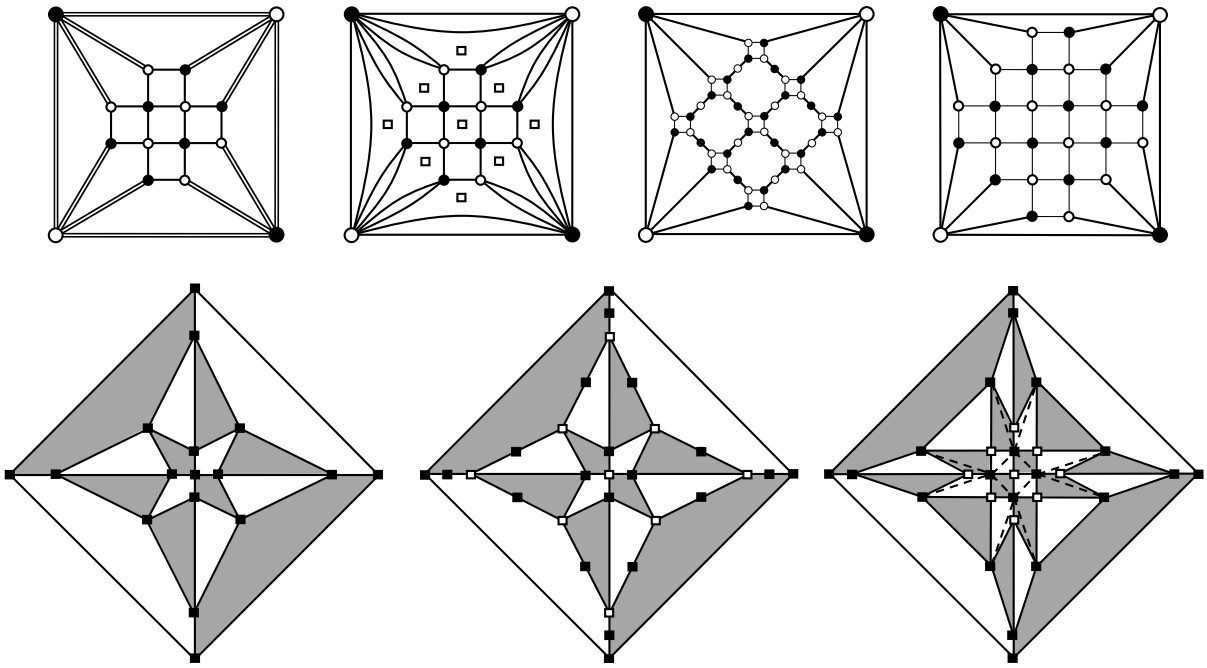

FIGURE 2. A sequence of updates leading from A'_4 to A'_5. Top row: graphs carrying the dimer model; double, thick and thin edges have weight 2, 1 and $\frac{1}{2}$, respectively. Bottom row: the same moves lead from the t-embedding $\mathcal{T}_3$ to $\mathcal{T}_4$; the last move (contraction of vertices of degree 2) removes dashed edges. Positions of urban renewals/central moves are indicated by white squares.

Let A'_{n+1}, the *reduced Aztec diamond* of size $n+1$, be obtained from A_{n+1} by the following sequence of moves (see Fig. 1):

(1) contract the vertices (p, q) of A_{n+1} with $p + q = n$, call w_{NE} the new (white) vertex; contract the vertices (p, q) of A_{n+1} with $p + q = -n$ to a new vertex w_{SW};
(2) similarly, contract the vertices (p, q) of A_{n+1} with $q - p = \pm n$ to new vertices b_{NW}, b_{SE};
(3) merge pairwise all the $4n$ pairs of parallel edges obtained during the first two steps.

By construction, the reduced Aztec diamond A'_{n+1} is composed of A_{n-1} and four additional 'boundary' vertices w_{NE}, b_{NW}, w_{SW} and b_{SE}, which can be thought of as located at positions $(\pm n, \pm n)$. The vertex w_{NE} is connected to all vertices on the north-east boundary of A_{n-1} as well as to b_{NW} and b_{SE} (and similarly for other boundary vertices). All edges of A'_{n+1} adjacent to boundary vertices have weight 2 while all other edges keep weight 1.

Clearly, the *faces* (except the outer one) of the reduced Aztec diamond A'_{n+1} of size $n + 1$ can be naturally indexed by pairs $(j, k) \in \mathbb{Z}^2$ such that $|j| + |k| < n$; see Fig. 1.

We now describe how one can recursively construct reduced Aztec diamonds using the local transforms listed above. To initialize the procedure, note that the reduced Aztec diamond A'_2 is a square formed by four outer vertices, with all edges having weight 2. To pass from A'_{n+1} to A'_{n+2}, one uses the following operations (see Fig. 2):

(1) split all edges adjacent to boundary vertices into pairs of parallel edges of weight 1;
(2) perform the urban renewal moves with those faces of A'_{n+1} for which $j + k + n$ is odd as shown on Fig. 2; note that the new vertical and horizontal edges have weight $\frac{1}{2}$;
(3) contract all vertices of degree 2; note that now all edges adjacent to boundary faces have weight 1 while all other edges have weight $\frac{1}{2}$;
(4) multiply all edge weights by 2 (this is a trivial gauge transformation).

2.2. **Symmetric t-embeddings (aka Coulomb gauges) of reduced Aztec diamonds.** We now recall the construction introduced in [16] under the name *Coulomb gauges* and discussed in [6, 7] under the name *t-embeddings*; we refer to these papers for more details.

Definition 2.1. Let $\mathcal{G}$ be a weighted planar bipartite graph and ν_{bw} denote the edge weights, where b and w stand for adjacent black and white vertices of $\mathcal{G}$, respectively. Let f be an inner face of G of degree $2d$ with vertices denoted by $w_1, b_1, \dots, w_d, b_d$ in counterclockwise order; we set $w_{d+1} := w_1$. *The X variable* associated with f is defined as

$$X_f \;:=\; \prod_{k=1}^{d} \frac{\nu_{b_k w_k}}{\nu_{b_k w_{k+1}}}\,.$$

Given a finite weighted planar bipartite graph $\mathcal{G}$ with a marked 'outer' face f_{out}, let $\mathcal{G}^*$ denote the *augmented dual* graph to $\mathcal{G}$, constructed as follows (see Fig. 2):

- to each inner face of $\mathcal{G}$, a vertex of $\mathcal{G}^*$ is associated;
- $\deg f_{\mathrm{out}}$ vertices are associated to the outer face f_{out} of $\mathcal{G}$;
- to each edge of $\mathcal{G}$, a dual edge of $\mathcal{G}^*$ is associated;
- an additional cycle of length $\deg f_{\mathrm{out}}$ connecting the outer vertices is included into $\mathcal{G}^*$ (note that this cycle is not included into the graph $\mathcal{G}^*$ in the notation of [7]).

Definition 2.2. A *t-embedding* of a finite weighted planar bipartite graph $\mathcal{G}$ is an embedding $\mathcal{T} : \mathcal{G}^* \to \mathbb{C}$ of its augmented dual $\mathcal{G}^*$ such that the following conditions are satisfied:

- under the embedding $\mathcal{T}$, the edges of $\mathcal{G}^*$ are non-degenerate straight segments, the faces are convex and do not overlap; the outer face of $\mathcal{T}(\mathcal{G}^*)$ corresponds to f_{out};
- angle condition: for each inner vertex v^* of $\mathcal{T}(\mathcal{G}^*)$, the sum of the angles at the corners corresponding to black faces is equal to π (and similarly for white faces);
- moreover, for each inner face of $\mathcal{G}$, if v^* denotes the corresponding dual vertex in $\mathcal{G}^*$ with neighbors $v_1^*, \dots, v_{2d}^*$ such that the (dual) edge $v^* v_{2k-1}^*$ is dual to the edge $w_k b_k$ of $\mathcal{G}$ and $v^* v_{2k}^*$ is dual to the edge $b_k w_{k+1}$ (as above, we assume that $w_1, b_1, \dots, w_k, b_k$ are listed in counterclockwise order and $w_{d+1} := w_1$), then we have

$$X_f \;=\; (-1)^{d+1} \prod_{k=1}^{d} \frac{\mathcal{T}(v^*) - \mathcal{T}(v_{2k-1}^*)}{\mathcal{T}(v_{2k}^*) - \mathcal{T}(v^*)}\,. \tag{2.1}$$

It is worth noting that the equation (2.1) implies that the *geometric* weights (dual edge lengths) $|\mathcal{T}(v^*) - \mathcal{T}(v_j^*)|$ are gauge equivalent to ν_{bw}. Therefore, in order to study the bipartite dimer model on an *abstract* planar graph $\mathcal{G}$ one can first find a Coulomb gauge/t-embedding of this graph and then consider the bipartite dimer model on this embedding with geometric weights. In our paper we apply this general philosophy to (reduced) Aztec diamonds A'_{n+1}.

Remark 2.3. In [6], the notion of a *perfect* t-embedding or simply *p-embeddings* of finite graphs is introduced. The additional condition required at boundary vertices of $\mathcal{T}(\mathcal{G}^*)$ is that the outer face is a tangential polygon and that, for all outer vertices, the inner edges of $\mathcal{T}(\mathcal{G}^*)$ are bisectors of the corresponding angles (in other words, the lines containing these edges pass through the center of the inscribed circle). In particular, the symmetric t-embeddings of reduced Aztec diamonds are perfect.

It was shown in [16] that, if $\mathcal{G}$ is a planar graph with outer face of degree 4 and if we prescribe the four outer vertices of $\mathcal{G}^*$ to be mapped to the four vertices of a given convex quadrilateral, then there exist two (potentially equal) t-embeddings of G with these prescribed boundary conditions. To respect the symmetries of the reduced Aztec diamonds A'_{n+1}, we will study their t-embeddings $\mathcal{T}_n$ with symmetric boundary conditions. Namely, if v_E^*, v_N^*, v_W^* and v_S^* denote the four outer vertices of the augmented dual to A'_{n+1}, then we require

$$\mathcal{T}_n(v_E^*) = 1, \qquad \mathcal{T}_n(v_N^*) = i, \qquad \mathcal{T}_n(v_W^*) = -1, \qquad \mathcal{T}_n(v_S^*) = -i; \tag{2.2}$$

see Fig. 3 for t-embeddings $\mathcal{T}_1$, $\mathcal{T}_2$, $\mathcal{T}_3$ of reduced Aztec diamonds A'_2, A'_3, A'_4 satisfying (2.2). As explained in [16], the notion of Coulomb gauges/t-embeddings is fully compatible with the

local moves in the dimer model. Therefore, we can inductively construct t-embeddings of the reduced Aztec diamond A'_{n+1} with boundary conditions (2.2) starting with that of A'_2. It is easy to see that the boundary conditions (2.2) yield $\mathcal{T}_1(0,0) = 0$. In particular, this implies that (2.2) defines a t-embedding of A'_{n+1} uniquely.

Recall that the faces of A'_{n+1} are labeled by pairs $(j,k) \in \mathbb{Z}^2$ such that $|j| + |k| < n$ and that we denote by $\mathcal{T}_n$ the t-embedding of the reduced Aztec diamond A'_{n+1}.

Proposition 2.4. *For each $n \geq 1$, the t-embeddings $\mathcal{T}_{n+1}$ and $\mathcal{T}_n$ of the reduced Aztec diamonds A'_{n+2} and A'_{n+1} are related as follows. The positions $\mathcal{T}_{n+1}(j,k)$ are given by*

(1) if $\{|j|,|k|\} = \{0,n\}$, then

$$\mathcal{T}_{n+1}(-n,0) = \tfrac{1}{2}(\mathcal{T}_n(-n+1,0) + \mathcal{T}_n(v^*_W)), \quad \mathcal{T}_{n+1}(0,n) = \tfrac{1}{2}(\mathcal{T}_n(0,n-1) + \mathcal{T}_n(v^*_N)),$$
$$\mathcal{T}_{n+1}(0,-n) = \tfrac{1}{2}(\mathcal{T}_n(0,-n+1) + \mathcal{T}_n(v^*_S)), \quad \mathcal{T}_{n+1}(n,0) = \tfrac{1}{2}(\mathcal{T}_n(n-1,0) + \mathcal{T}_n(v^*_E));$$

(2) if $1 \leq j \leq n-1$ and $k = n-j$, then

$$\mathcal{T}_{n+1}(j,n-j) = \tfrac{1}{2}(\mathcal{T}_n(j-1,n-j) + \mathcal{T}_n(j,n-j-1))$$

and similarly for $\mathcal{T}_{n+1}(-j,j-n)$, $\mathcal{T}_{n+1}(-j,n-j)$ and $\mathcal{T}_{n+1}(j,j-n)$;

(3) if $|j| + |k| < n$ and $j+k+n$ is even, then $\mathcal{T}_{n+1}(j,k) = \mathcal{T}_n(j,k)$;

(4) if $|j| + |k| < n$ and $j+k+n$ is odd, then

$$\mathcal{T}_{n+1}(j,k) = \tfrac{1}{2}(\mathcal{T}_{n+1}(j+1,k) + \mathcal{T}_{n+1}(j-1,k) + \mathcal{T}_{n+1}(j,k+1) + \mathcal{T}_{n+1}(j,k-1)) - \mathcal{T}_n(j,k).$$

Proof. When constructing the reduced Aztec diamond A'_{n+2} from A'_{n+1} following the procedure described in Section 2.1, the first step is to split edges of A'_{n+1} that are adjacent to boundary vertices into two parallel edges of equal weight. This amounts to adding the midpoints of the corresponding edges of $\mathcal{T}_n$ to the t-embedding, i.e., to (1) and (2); see the first step in Fig. 2.

Further, (3) reflects the fact that, for $j+k+n$ even, the inner faces (j,k) of $\mathcal{T}_n$ are not destroyed by urban renewal moves and hence the positions of the corresponding dual vertices in the t-embedding $\mathcal{T}_{n+1}$ remain the same as in $\mathcal{T}_n$; see Fig. 2.

Finally, (4) follows from the explicit description of the urban renewal procedure in terms of the t-embedding, which is called the central (or Miquel) move in [16, Section 5]. In general, the position of $\mathcal{T}_{n+1}(j,k)$ is given by a *rational* function involving the positions, already known, of four neighbors $\mathcal{T}_{n+1}(j \pm 1,k)$, $\mathcal{T}_{n+1}(j,k \pm 1)$ and the position $\mathcal{T}_n(j,k)$. However, in our case we can additionally use the fact that $X_f = 1$ for all X variables assigned to faces at which the urban renewals are performed. Therefore, equation (2.1) implies that $\mathcal{T}_{n+1}(j,k)$ and $\mathcal{T}_n(j,k)$ are the two roots of the quadratic equation

$$(z - \mathcal{T}_{n+1}(j+1,k))(z - \mathcal{T}_{n+1}(j-1,k)) + (z - \mathcal{T}_{n+1}(j,k+1))(z - \mathcal{T}_{n+1}(j,k-1)) = 0.$$

The required *linear* expression for $\mathcal{T}_{n+1}(j,k)$ easily follows from Vieta's formula. □

2.3. **Origami maps associated to the t-embeddings of reduced Aztec diamonds.** To each t-embedding $\mathcal{T} : \mathcal{G}^* \to \mathbb{C}$ one can associate the so-called *origami map* $\mathcal{O} : \mathcal{G}^* \to \mathbb{C}$, defined up to a global translation and rotation. Informally speaking, this map can be constructed as follows: choose a reference white face w_0 of $\mathcal{T}(\mathcal{G}^*)$ and set $\mathcal{O}(v^*) := \mathcal{T}(v^*)$ for all vertices v^* of $\mathcal{G}^*$ adjacent to w_0. To find positions $\mathcal{O}(v^*)$ of vertices of $\mathcal{G}^*$ lying at distance 1 from w_0, glue copies of *conjugated* black faces adjacent to w_0 to the image $\mathcal{O}(w_0)$. Continue this procedure inductively by gluing copies of white (resp., black) faces of $\mathcal{T}(\mathcal{G}^*)$ to the already constructed part of $\mathcal{O}(\mathcal{G}^*)$, keeping (resp., reverting) their orientation and keeping the same adjacency relations between faces as in $\mathcal{T}(\mathcal{G}^*)$. The angle condition guarantees that this procedure is locally (and hence globally) consistent; see Fig. 3 for an example.

We refer the reader to [16] and [7, Section 2] for the formal definition of the origami map, note that this definition is also fully consistent with the local moves in the dimer model. In particular, an urban renewal move does not affect positions $\mathcal{O}(v^*)$ except that of the dual vertex

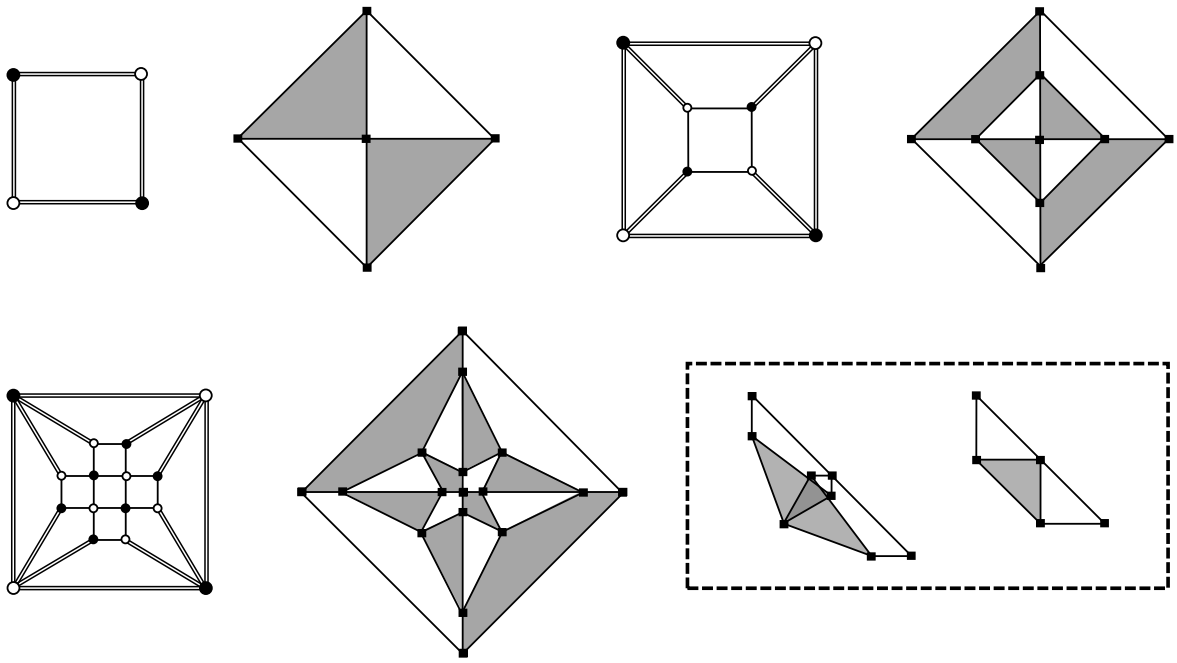

FIGURE 3. Reduced Aztec diamonds A'_2, A'_3, A'_4 and their symmetric t-embeddings $\mathcal{T}_1$, $\mathcal{T}_2$, $\mathcal{T}_3$. BOTTOM-RIGHT: illustration of the origami maps $\mathcal{O}_2$ and $\mathcal{O}_3$; the colors of faces inherit those from the north-east parts of $\mathcal{T}_2$ and $\mathcal{T}_3$. As discussed below (see Remark 2.8 and Eq. (3.4)), the images of the origami maps $\mathcal{O}_n$ are asymptotically one-dimensional for large n.

associated with the face of $\mathcal{G}$ at which this move is performed. Moreover, it is easy to see that the identity (2.1) and the angle condition imply that

$$X_f \;=\; (-1)^{d+1} \prod_{k=1}^{d} \frac{\mathcal{O}(v^*) - \mathcal{O}(v^*_{2k-1})}{\mathcal{O}(v^*_{2k}) - \mathcal{O}(v^*)}\,, \tag{2.3}$$

where we use the same notation as in (2.1). Therefore, the update rule for the origami map $\mathcal{O}$ under an urban renewal is exactly the same as the central move for $\mathcal{T}$.

Let $\mathcal{O}_n$ be the origami map associated to the t-embedding $\mathcal{T}_n$ of the reduced Aztec diamond A'_{n+1} constructed starting with the north-east outer face w_{NE} of $\mathcal{T}_n$. In other words, we start the iterative construction of $\mathcal{O}_n$ by declaring $\mathcal{O}_n(v^*_E) := \mathcal{T}_n(v^*_E) = 1$, $\mathcal{O}_n(v^*_N) := \mathcal{T}_n(v^*_N) = i$ and $\mathcal{O}_n(j, n-1-j) := \mathcal{T}_n(j, n-j-1)$ for all $0 \le j \le n-1$. It is easy to see that

$$\mathcal{O}_n(v^*_W) = \mathcal{O}_n(v^*_E) = 1 \quad \text{and} \quad \mathcal{O}_n(v^*_N) = \mathcal{O}_n(v^*_S) = i \tag{2.4}$$

for all $n \ge 1$ and that $\mathcal{O}_1(0,0) = 0$.

Proposition 2.5. *Let $n \ge 1$. The origami map $\mathcal{O}_{n+1}$ can be constructed from $\mathcal{O}_n$ using the same update rules (1)–(4) as in Proposition 2.4, with boundary conditions* (2.4) *instead of* (2.2).

Proof. The proof repeats that of Proposition 2.5. The least trivial update rule (4) for $\mathcal{O}_{n+1}$ follows from (2.3) in the same way as it follows from (2.1) for $\mathcal{T}_{n+1}$. □

2.4. **$\mathcal{T}_n$ and $\mathcal{O}_n$ as solutions to the discrete wave equation.** We now interpret the recurrence relations from Proposition 2.4 as a discrete wave equation in the cone $|j| + |k| < n$.

Denote by $\mathbb{Z}_+$ the set of all non-negative integers and by Λ^+ the cubic-centered half-space, that is the collection of all triples of integers $(j,k,n) \in \mathbb{Z}^2 \times \mathbb{Z}_+$ such that $j+k+n$ is *odd*. Let a function $f_0 : \Lambda^+ \to \mathbb{R}$ be defined by the following conditions:

(1) $f_0(j,k,0) = 0$ for all j and k (such that $j+k$ is odd);
$f_0(0,0,1) = 1$ and $f_0(j,k,1) = 0$ for all other pairs j,k (such that $j+k$ is even);

(2) for all $(j,k,n+1) \in \Lambda^+$ such that $n \geq 1$ we have

$$f_0(j,k,n+1) + f_0(j,k,n-1) \tag{2.5}$$
$$= \tfrac{1}{2}(f_0(j+1,k,n) + f_0(j-1,k,n) + f_0(j,k+1,n) + f_0(j,k-1,n)).$$

We call (2.5) the *discrete wave equation* and f_0 is the *fundamental solution* to this equation. To justify the name note that the formal subtraction of a (non-defined as $j+k+n$ has the wrong parity) term $2f(j,k,n)$ from both sides of (2.5) allows one to see it as a discretization of the two-dimensional wave equation $\partial_{tt}\psi = \frac{1}{2}(\partial_{xx}\psi + \partial_{yy}\psi)$.

Definition 2.6. Let b_0, b_E, b_N, b_W and b_S be five complex numbers. We say that a function $f : \Lambda^+ \to \mathbb{C}$ solves the *discrete wave equation in the cone* $|j|+|k| < n$ with boundary conditions $(b_0; b_E, b_N, b_W, b_S)$ if it satisfies the following properties:

(0) $f(j,k,n) = 0$ if $|j|+|k| \geq n$ (in particular, $f(j,k,0) = 0$ for all j,k);

(1) boundary condition at the tip of the cone: $f(0,0,1) = b_0$;

(2) boundary conditions at the edges: for each $n \geq 1$ we have

$$f(-n,0,n+1) = \tfrac{1}{2}(f(-n+1,0,n) + b_W), \quad f(0,n,n+1) = \tfrac{1}{2}(f(0,n-1,n) + b_N),$$
$$f(0,-n,n+1) = \tfrac{1}{2}(f(0,-n+1,n) + b_S), \quad f(n,0,n+1) = \tfrac{1}{2}(f(n-1,0,n) + b_E).$$

(Thus, $f(n,0,n+1) = 2^{-n}b_0 + (1-2^{-n})b_E$ and similarly at other edges of the cone.)

(3) discrete wave equation in the bulk of the cone and on its sides: for each $(j,k,n+1) \in \Lambda^+$ such that $n \geq 1$, $|j|+|k| \leq n$ and $\{|j|,|k|\} \neq \{0,n\}$, the identity (2.5) is satisfied. In particular, we require that $f(j,n-j,n+1) = \frac{1}{2}(f(j-1,n-j,n) + f(j,n-j-1,n))$ for all $1 \leq j \leq n-1$ and similarly on other sides of the cone.

It is easy to see that the above conditions define the function $f : \Lambda^+ \to \mathbb{C}$ uniquely. Moreover, the solution in the cone with boundary conditions $(1;0,0,0,0)$ is given by the fundamental solution f_0 in the half-space Λ^+. Denote by f_E the solution in the cone with boundary conditions $(0;1,0,0,0)$ and similarly for f_N, f_W and f_S. By linearity, a general solution in the cone with boundary conditions $(b_0; b_E, b_N, b_W, b_S)$ can be written as

$$f = b_0 f_0 + b_E f_E + b_N f_N + b_W f_W + b_S f_S.$$

The functions f_E, f_N, f_W and f_S represent the impact of a constant source moving in the east, north, west and south directions, respectively, and thus can be expressed via f_0. In particular,

$$f_E(j,k,n) = \frac{1}{2}\sum_{s=1}^{n-1} f_0(j-s,k,n-s) \tag{2.6}$$

and similarly for f_N, f_W and f_S.

Proposition 2.7. *For all $n \geq 1$, the values $\mathcal{T}_n(j,k)$ for $j+k+n$ odd are given by the solution to the discrete wave equation in the cone $|j|+|k| < n$ with boundary conditions $(0;1,i,-1,-i)$.*

Similarly, the values $\mathcal{O}_n(j,k)$ for $j+k+n$ odd are given by the solution to the discrete wave equation in the cone $|j|+|k| < n$ with boundary conditions $(0;1,i,1,i)$.

If $|j|+|k| < n$ and $j+k+n$ is even, then $\mathcal{T}_n(j,k) = \mathcal{T}_{n-1}(j,k)$ and $\mathcal{O}_n(j,k) = \mathcal{O}_{n-1}(j,k)$.

Proof. This is a straightforward reformulation of recurrence relations from Proposition 2.4. □

Remark 2.8. Let

$$\mathcal{O}'_n := e^{i\frac{\pi}{4}}(\tfrac{1}{2}(1+i) - \mathcal{O}_n)$$

be another version of the origami map (recall that $\mathcal{O}_n$ is defined up to a global translation and rotation). It is easy to see that $\sqrt{2}\,\mathrm{Im}(\mathcal{O}'_n(j,k)) = f_0(j,k,n)$ and that the values $\sqrt{2}\,\mathrm{Re}(\mathcal{O}'_n(j,k))$ are given by the solution to the wave equation in the cone with boundary conditions $(0;1,-1,1,-1)$, provided that $j+k+n$ is odd.

3. The limit of t-embeddings and the Aztec conformal structure

Recall that the equation (2.5) can be viewed as a discretization of the wave equation

$$\partial_{tt}\psi \;=\; \tfrac{1}{2}(\partial_{xx}\psi + \partial_{yy}\psi). \tag{3.1}$$

The continuous counterpart $2\psi_0$ of the fundamental solution f_0 satisfies boundary conditions $\psi_0\big|_{t=0} = 0$, $\partial_t\psi_0\big|_{t=0} = \delta_{(0,0)}$, the factor 2 comes from the area of the horizontal plaquette with vertices $(\pm 1, 0, 0)$, $(0, \pm 1, 0)$. Therefore,

$$\psi_0(x,y,t) = \frac{1}{\pi}\begin{cases}(t^2 - 2x^2 - 2y^2)^{-\frac{1}{2}} & \text{if } x^2+y^2 < \frac{1}{2}t^2,\\ 0 & \text{otherwise.}\end{cases} \tag{3.2}$$

The continuous counterpart of the function (2.6) is thus given by a *self-similar* solution

$$\psi_E(x,y,t) \;=\; \int_0^t \psi_0(x-s, y, t-s)ds \;=:\; \psi_E^{(1)}(x/t, y/t)$$

to the wave equation (3.1) with a *super-sonic* source moving with speed 1 in the east direction. In particular,

$$\psi_E^{(1)}(x,y) \;=\; \begin{cases}1 & \text{if } \;(x,y)\in \diamondsuit \smallsetminus \overline{\mathbb{D}}_\diamondsuit \;\text{ and }\; x > \frac{1}{2},\\ 0 & \text{if } \;(x,y)\in \diamondsuit \smallsetminus \overline{\mathbb{D}}_\diamondsuit \;\text{ and }\; x < \frac{1}{2},\end{cases} \tag{3.3}$$

where $\diamondsuit = \{(x,y)\in\mathbb{R}^2 \cong \mathbb{C} : |x| + |y| < 1\}$ and $\mathbb{D}_\diamondsuit = \frac{\sqrt{2}}{2}\mathbb{D} \subset \diamondsuit$. Below we take for granted the following two facts:

- The discrete fundamental solution f_0 uniformly (in j,k) decays in time:
$$\max_{j,k:(j,k,n)\in\Lambda^+} f_0(j,k,n) = o(1) \quad \text{as} \quad n\to\infty; \tag{3.4}$$
- The function f_E (and similarly for f_N, f_W and f_S) has the following asymptotics:
$$f_E(j,k,n) = \psi_E^{(1)}(j/n, k/n) + o(1) \quad \text{as} \quad n\to\infty, \tag{3.5}$$
uniformly over $(j/n, k/n)$ on compact subsets of $\diamondsuit$.

Though we were unable to find an explicit reference, we feel that providing rigorous proofs of (3.4) and (3.5) goes beyond the scope of this short note. Since many techniques for the analysis of the discrete wave equation on Λ^+ are available (e.g., Fourier transform and saddle point methods, cf. [9]), we believe that such proofs should not be very hard to obtain.

We now consider the mapping

$$\begin{aligned}(x,y)\in\mathbb{D}_\diamondsuit \quad &\mapsto \quad (z(x,y), \vartheta(x,y)) \in \diamondsuit\times\mathbb{R};\\ z(x,y) \;&:=\; \psi_E^{(1)}(x,y) + i\psi_N^{(1)}(x,y) - \psi_W^{(1)}(x,y) - i\psi_S^{(1)}(x,y),\\ \vartheta(x,y) \;&:=\; \tfrac{\sqrt{2}}{2}(\psi_E^{(1)}(x,y) - \psi_N^{(1)}(x,y) + \psi_W^{(1)}(x,y) - \psi_S^{(1)}(x,y)),\end{aligned} \tag{3.6}$$

let us emphasize that $z(x,y)\neq x+iy$. It is worth noting that this mapping is also well-defined on the whole set $\diamondsuit$. Due to (3.3), it sends the four connected regions of $\diamondsuit\smallsetminus\mathbb{D}_\diamondsuit$ (which correspond to four frozen regions of Aztec diamonds) to the four *points* $(\pm 1, 1/\sqrt{2})$ and $(\pm i, -1/\sqrt{2})$.

Recall that $\mathcal{T}_n$ denotes the t-embedding of the reduced Aztec diamond A'_{n+1} and that $\mathcal{O}'_n$ is a version of the origami map associated to $\mathcal{T}_n$ introduced in Remark 2.8. Proposition 2.7 and (3.4), (3.5) give

$$\mathcal{T}_n(j,k) \;=\; z(j/n,k/n) + o(1), \qquad \begin{aligned}\mathrm{Re}(\mathcal{O}'_n(j,k)) \;&=\; \vartheta(j/n,k/n) + o(1),\\ \mathrm{Im}(\mathcal{O}'_n(j,k)) \;&=\; o(1)\end{aligned}$$

as $n\to\infty$, uniformly over j/n and k/n on compact subsets of $\diamondsuit$.

It is not hard to find an explicit expression for $z(x,y)$ and $\vartheta(x,y)$. To this end, introduce the polar coordinates (r,ϕ) in the plane (x,y). A straightforward computation shows that each self-similar solution $\psi^{(1)}(x/t, y/t)$ of the wave equation (3.1) satisfies

$$\left[(1-2r^2)\partial_{rr} + \left(\frac{1}{r} - 4r\right)\partial_r + \frac{1}{r^2}\partial_{\phi\phi}\right]\psi^{(1)}(x,y) \;=\; 0. \tag{3.7}$$

This equation can be viewed as the harmonicity condition provided an appropriate change of the radial variable is made. Namely, let

$$\zeta(x,y) := e^{i\phi(x,y)}\rho(x,y) \in \mathbb{D} \quad \text{for} \quad (x,y) \in \mathbb{D}_\diamondsuit,$$

where the new radial variable $\rho = \rho(x,y)$ is defined by (1.1). (Note that in our context this change of variables naturally appears from the 2D wave equation and not from any a priori knowledge on the dimer model.) It is straightforward to check that (3.7) can be written as

$$\frac{\rho^2}{r^2}\Delta_{(\rho,\phi)}\psi^{(1)} \;=\; \frac{\rho^2}{r^2}\Big[\frac{1}{\rho}\partial_\rho(\rho\partial_\rho) + \frac{1}{\rho^2}\partial_{\phi\phi}\Big]\psi^{(1)} \;=\; 0.$$

Thus, both functions z and ϑ are harmonic in the variable ζ and hence can be written in terms of their boundary values. Let $\mathrm{hm}_\mathbb{D}(\cdot,\gamma)$ be the harmonic measure of a boundary arc $\gamma \subset \partial\mathbb{D}$. We have

$$z(x,y) = \mathrm{hm}_\mathbb{D}(\zeta(x,y);\gamma_E) + i\,\mathrm{hm}_\mathbb{D}(\zeta(x,y);\gamma_N) - \mathrm{hm}_\mathbb{D}(\zeta(x,y);\gamma_W) - i\,\mathrm{hm}_\mathbb{D}(\zeta(x,y);\gamma_S),$$

$$\vartheta(x,y) = \tfrac{\sqrt{2}}{2}\big(\,\mathrm{hm}_\mathbb{D}(\zeta(x,y);\gamma_E) - \mathrm{hm}_\mathbb{D}(\zeta(x,y);\gamma_N) + \mathrm{hm}_\mathbb{D}(\zeta(x,y);\gamma_W) - \mathrm{hm}_\mathbb{D}(\zeta(x,y);\gamma_S)\big),$$

where $\gamma_E := (e^{-i\frac{\pi}{4}}, e^{i\frac{\pi}{4}})$, $\gamma_N := (e^{i\frac{\pi}{4}}, e^{i\frac{3\pi}{4}})$, $\gamma_W := (e^{i\frac{3\pi}{4}}, e^{i\frac{5\pi}{4}})$ and $\gamma_S := (e^{i\frac{5\pi}{4}}, e^{i\frac{7\pi}{4}})$ denote four boundary arcs of the unit disc $\mathbb{D}$. Recall that, if $\alpha < \beta < \alpha + 2\pi$, then

$$\mathrm{hm}_\mathbb{D}(\zeta;(e^{i\alpha},e^{i\beta})) \;=\; \tfrac{1}{\pi}\big(\arg(e^{i\beta}-\zeta) - \arg(e^{i\alpha}-\zeta)\big) - \tfrac{1}{2\pi}(\beta-\alpha)\,. \tag{3.8}$$

Note that $(x,y) \mapsto \zeta(x,y)$ is an orientation preserving diffeomorphism of $\mathbb{D}_\diamondsuit$ and $\mathbb{D}$. From the explicit formula for $z(x,y)$ and the argument principle, it is also clear that $\zeta \mapsto z$ is an orientation preserving diffeomorphism of $\mathbb{D}$ and $\diamondsuit$. In particular, it makes sense to view $\vartheta = \vartheta(x,y)$ as a function of $z = z(x,y) \in \diamondsuit$. Since each of the origami maps $\mathcal{O}_n$ does not increase distances comparing to those in $\mathcal{T}_n$, the same should hold true in the limit as $n \to \infty$. Therefore, the function $z \mapsto \vartheta$ is 1-Lipschitz.

Following the approach developed in [6, 7], we now consider the surface $(z(x,y),\vartheta(x,y))$ as embedded into the *Minkowski* (or Lorentz) space $\mathbb{R}^{2+1}$ rather than into the usual Euclidean space $\mathbb{R}^3$. The Lipschitzness condition discussed above implies that this surface is space-like. We are now ready to formulate the most conceptual observation of this note. Let $\mathrm{C}_\diamondsuit$ be a (non-planar) quadrilateral in $\mathbb{R}^2 \times \mathbb{R} \cong \mathbb{C} \times \mathbb{R}$ with vertices

$$\mathrm{C}_\diamondsuit: \quad (1,\tfrac{\sqrt{2}}{2}) \;—\; (i,-\tfrac{\sqrt{2}}{2}) \;—\; (-1,\tfrac{\sqrt{2}}{2}) \;—\; (-i,-\tfrac{\sqrt{2}}{2}) \;—\; (1,\tfrac{\sqrt{2}}{2}). \tag{3.9}$$

Proposition 3.1. *The surface* $\mathrm{S}_\diamondsuit := \{(z(x,y),\vartheta(x,y)),\ (x,y) \in \mathbb{D}_\diamondsuit\}$ *is a minimal surface in the Minkowski (or Lorentz) space* $\mathbb{R}^{2+1}$*, whose boundary is given by* $\mathrm{C}_\diamondsuit$*; see Fig. 5. Moreover, the variable* $\zeta(x,y) \in \mathbb{D}$ *provides the conformal parametrization of this minimal surface.*

Proof. From now onwards we view z and ϑ as functions of the variable $\zeta = \zeta(x,y) \in \mathbb{D}$ rather than those of $(x,y) \in \mathbb{D}_\diamondsuit$. Let us first discuss the boundary behavior of the mapping $\zeta \mapsto (z,\vartheta)$. From the explicit formulas, it is clear that $(z(\zeta),\vartheta(\zeta)) \to (1,\frac{\sqrt{2}}{2})$ if ζ approaches the boundary arc γ_E, and similarly for the three other arcs. Near the point $\zeta = e^{i\frac{\pi}{4}}$ separating γ_E and γ_N one observes the following behavior:

$$\begin{aligned} z(\zeta) &= \tfrac{1+i}{2} + \tfrac{1-i}{\pi}\big(\arg(e^{i\frac{\pi}{4}}-\zeta) - \tfrac{\pi}{4}\big) + O(|\zeta - e^{i\frac{\pi}{4}}|),\\ \vartheta(\zeta) &= \tfrac{\sqrt{2}}{\pi}\big(\arg(e^{i\frac{\pi}{4}}-\zeta) - \tfrac{\pi}{4}\big) + O(|\zeta - e^{i\frac{\pi}{4}}|), \end{aligned}$$

where the branch of arg is chosen so that $\arg(e^{i\frac{\pi}{4}} - \zeta) \in (-\frac{\pi}{4}, \frac{3\pi}{4})$ for $\zeta \in \mathbb{D}$. This means that ϑ and z are almost linearly dependent near the point $e^{i\frac{\pi}{4}}$ and thus the boundary of the surface $\mathrm{S}_\diamondsuit$ contains the full segment with endpoints $(1,\frac{\sqrt{2}}{2})$ and $(i,-\frac{\sqrt{2}}{2})$. Repeating the same argument for each of the four points separating the arcs γ_E, γ_N, γ_W and γ_S, we conclude that the boundary of $\mathrm{S}_\diamondsuit$ is given by (3.9).

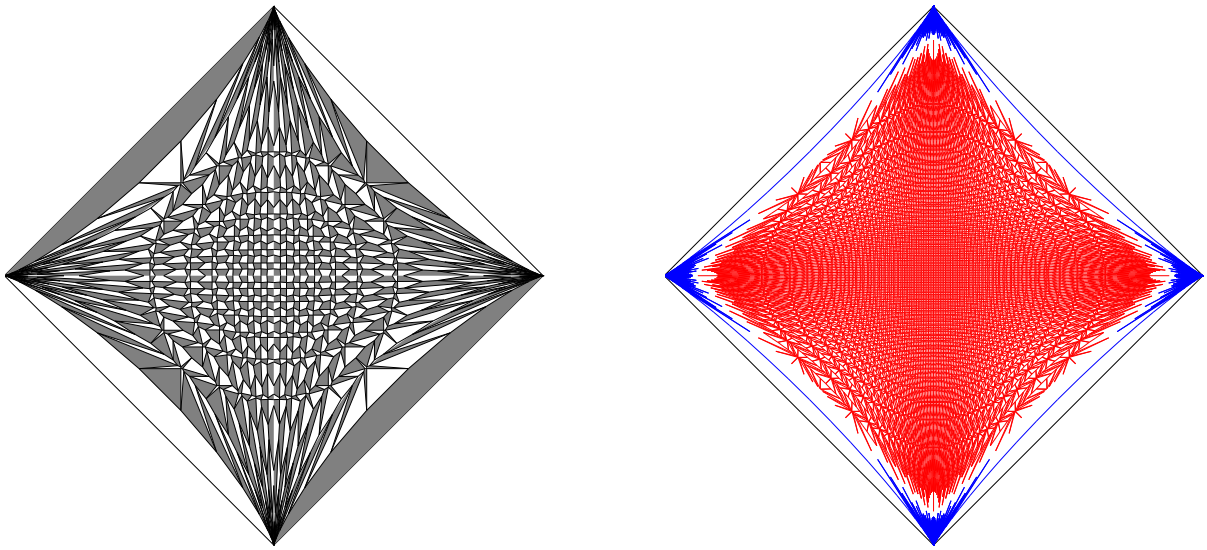

FIGURE 4. LEFT: symmetric t-embedding of the reduced Aztec diamond A'_{27}. RIGHT: t-embedding $\mathcal{T}_{101}$ of the reduced Aztec diamond A'_{102}, the edges connecting $\mathcal{T}_{101}(j_1, k_1)$ and $\mathcal{T}_{101}(j_2, k_2)$ are colored *red* if both $(j_{1,2}^2 + k_{1,2}^2) \le 0.49 \cdot 10^4$, *blue* if both $(j_{1,2}^2 + k_{1,2}^2) \ge 0.5 \cdot 10^4$, and are not shown otherwise.

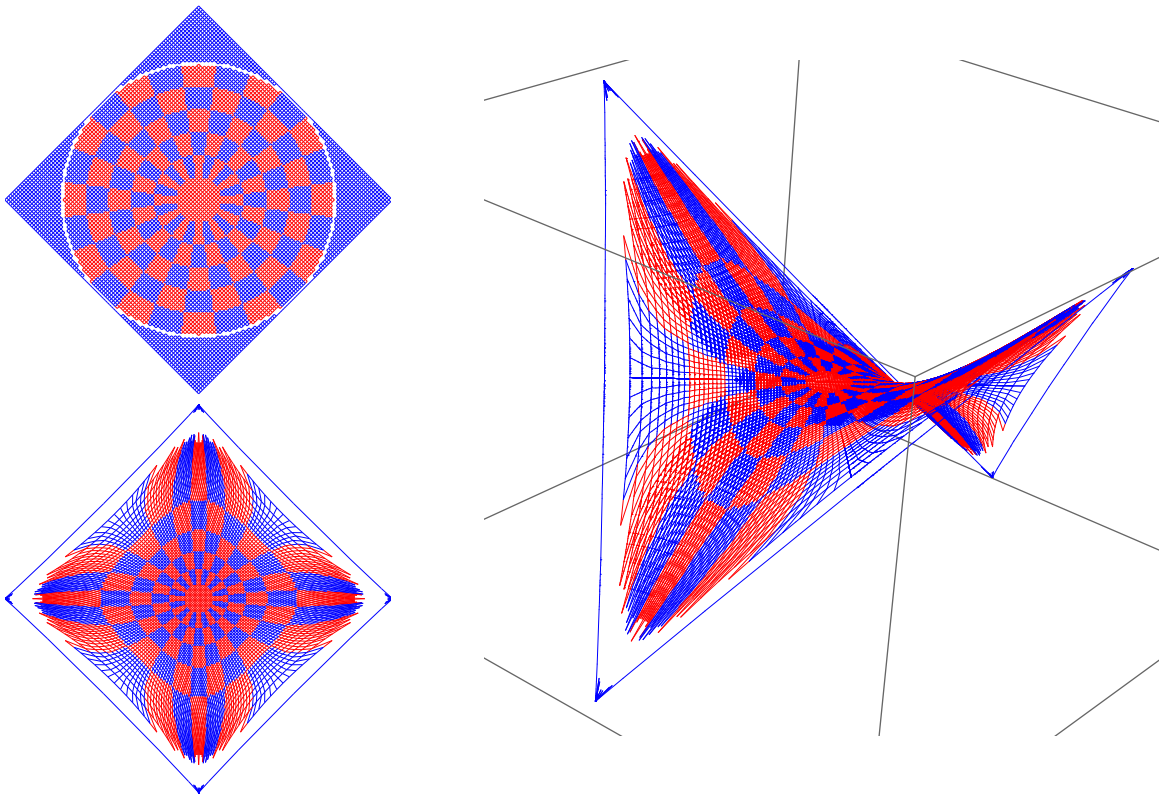

FIGURE 5. TOP-LEFT: the grid of points $(\frac{1}{1600}j, \frac{1}{1600}k)$, $j, k \in 16\mathbb{Z}$, $j + k \in 32\mathbb{Z}$. The additional red-blue coloring of the liquid region is introduced for visibility. BOTTOM-LEFT: The image of this grid under the mapping $\mathcal{T}_{1601}$. Four frozen zones of A'_{1602} are collapsed to tiny vicinities of the corners; the image of a thin white vicinity of the arctic circle is stretched in a square-root fashion. RIGHT: The grid of points $(\mathcal{T}_{1601}(j,k), \mathcal{O}'_{1601}(j,k))$, $j, k \in 16\mathbb{Z}$, $j + k \in 32\mathbb{Z}$, approximates the Lorentz-minimal surface $\mathrm{S}_\diamondsuit$ spanning the contour $\mathrm{C}_\diamondsuit \subset \mathbb{R}^{2+1}$.

We now prove that ζ is a *conformal* parametrization of $\mathrm{S}_\diamondsuit$; recall that angles on the surface $\mathrm{S}_\diamondsuit$ are measured with respect to the Lorentz metric in $\mathbb{R}^{2+1}$. To this end, we need to show that

$$(\partial_\zeta z)(\zeta)\cdot(\partial_\zeta \overline{z})(\zeta) \;=\; ((\partial_\zeta \vartheta)(\zeta))^2 \quad \text{for} \quad \zeta\in\mathbb{D}, \tag{3.10}$$

where $\partial_\zeta = \frac{1}{2}(\partial_{\mathrm{Re}\zeta} - i\partial_{\mathrm{Im}\zeta})$ stands for the Wirtinger derivative with respect to the variable ζ. Recall that the functions $z(\zeta)$ and $\vartheta(\zeta)$ are explicit linear combinations of the harmonic measures of the arcs γ_E, γ_N, γ_W, γ_S. From (3.8), one easily sees that

$$\partial_\zeta \,\mathrm{hm}_{\mathbb{D}}(\zeta;(e^{i\alpha},e^{i\beta})) \;=\; \tfrac{i}{2\pi}\big((\zeta-e^{i\beta})^{-1}-(\zeta-e^{i\alpha})^{-1}\big)\,.$$

Therefore, the equation (3.10) is equivalent to the identity

$$\begin{aligned}
&\big((1-i)(\zeta-e^{i\frac{\pi}{4}})^{-1}+(1+i)(\zeta-e^{i\frac{3\pi}{4}})^{-1}+(-1+i)(\zeta-e^{i\frac{5\pi}{4}})^{-1}+(-1-i)(\zeta-e^{i\frac{7\pi}{4}})^{-1}\big)\\
\times&\big((1+i)(\zeta-e^{i\frac{\pi}{4}})^{-1}+(1-i)(\zeta-e^{i\frac{3\pi}{4}})^{-1}+(-1-i)(\zeta-e^{i\frac{5\pi}{4}})^{-1}+(-1+i)(\zeta-e^{i\frac{7\pi}{4}})^{-1}\big)\\
&\qquad=\; 2\big((\zeta-e^{i\frac{\pi}{4}})^{-1}-(\zeta-e^{i\frac{3\pi}{4}})^{-1}+(\zeta-e^{i\frac{5\pi}{4}})^{-1}-(\zeta-e^{i\frac{7\pi}{4}})^{-1}\big)^2\,,
\end{aligned}$$

which is straightforward to check.

Finally, both z and ϑ are *harmonic* functions in the conformal (provided that the intrinsic metric on $\mathrm{S}_\diamondsuit$ is induced from $\mathbb{R}^{2+1}$) parametrization ζ of the space-like surface $\mathrm{S}_\diamondsuit$. Classically, this implies that $\mathrm{S}_\diamondsuit$ is minimal in the metric of $\mathbb{R}^{2+1}$. □

4. Numerical simulations

The discrete wave equation (2.5) trivially admits very fast simulations, a few examples are given in Fig. 4 and Fig. 5. Actually, constructing solutions to (2.5) is more memory-consuming than time-consuming if one wants to keep all binary digits so as not to loose control over cancellations, inherent to the wave equation in 2D. The pictures in Fig. 4 and, notably, in Fig. 5 are obtained by such *exact* simulations.

5. Conclusion

In this note we studied the symmetric t-embeddings $\mathcal{T}_n$ (or Coulomb gauges) of homogeneous Aztec diamonds A_n and tested the framework developed in [6, 7] on this classical example of the dimer model that leads to a non-trivial conformal structure of the fluctuations. Both analytic arguments and numerical simulations strongly indicate the convergence of the graphs $(\mathcal{T}_n,\mathcal{O}_n)$ of the corresponding origami maps $\mathcal{O}_n$ to a Lorentz-minimal surface $\mathrm{S}_\diamondsuit$ embedded into the Minkowski (or Lorentz) space $\mathbb{R}^{2+1}$. The intrinsic conformal structure of $\mathrm{S}_\diamondsuit$ provides a new description of the well-studied scaling limit of dimer fluctuations in the liquid regions of A_n. Though additional work should be done to get a new rigorous proof of the convergence of fluctuations (see Remark 1.1), our results strongly support the paradigm of [6, 7].

Acknowledgements. This research was partially supported by the ANR-18-CE40-0033 project DIMERS. We would like to thank Benoît Laslier and Marianna Russkikh for many discussions and comments on draft versions of this note, and Jesper Lykke Jacobsen, Gregg Musiker and Istvan Prause for pointing out relevant references. D.C. is grateful to Olivier Biquard for helpful comments on Lorentz-minimal surfaces. S.R. thanks the Fondation Sciences Mathématiques de Paris for the support during the academic year 2018/19.

References

[1] Niklas C. Affolter. Miquel Dynamics, Clifford Lattices and the Dimer Model. *arXiv e-prints*, page arXiv:1808.04227, Aug 2018.

[2] Nicolas Allegra, Jérôme Dubail, Jean-Marie Stéphan, and Jacopo Viti. Inhomogeneous field theory inside the arctic circle. *J. Stat. Mech. Theory Exp.*, (5):053108, 76, 2016.

[3] D. Betea, C. Boutillier, J. Bouttier, G. Chapuy, S. Corteel, and M. Vuletić. Perfect sampling algorithms for Schur processes. *Markov Process. Related Fields*, 24(3):381–418, 2018.

[4] Mireille Bousquet-Mélou, James Propp, and Julian West. Perfect matchings for the three-term Gale-Robinson sequences. *Electron. J. Combin.*, 16(1):Research Paper 125, 37, 2009.

[5] Alexey Bufetov and Vadim Gorin. Fluctuations of particle systems determined by Schur generating functions. *Adv. Math.*, 338:702–781, 2018.
[6] Dmitry Chelkak, Benoít Laslier, and Marianna Russkikh. Bipartite dimer model: p-embeddings and Lorentz-minimal surfaces. In preparation, 2020.
[7] Dmitry Chelkak, Benoît Laslier, and Marianna Russkikh. Dimer model and holomorphic functions on t-embeddings of planar graphs. *arXiv e-prints*, page arXiv:2001.11871, Jan 2020.
[8] Sunil Chhita, Kurt Johansson, and Benjamin Young. Asymptotic domino statistics in the Aztec diamond. *Ann. Appl. Probab.*, 25(3):1232–1278, 2015.
[9] Henry Cohn, Noam Elkies, and James Propp. Local statistics for random domino tilings of the Aztec diamond. *Duke Math. J.*, 85(1):117–166, 1996.
[10] Noam Elkies, Greg Kuperberg, Michael Larsen, and James Propp. Alternating-sign matrices and domino tilings. I. *J. Algebraic Combin.*, 1(2):111–132, 1992.
[11] Noam Elkies, Greg Kuperberg, Michael Larsen, and James Propp. Alternating-sign matrices and domino tilings. II. *J. Algebraic Combin.*, 1(3):219–234, 1992.
[12] Vadim Gorin. Lectures on random tilings. `http://math.mit.edu/vadicgor/Random_tilings.pdf`, 2019.
[13] Etienne Granet, Louise Budzynski, Jérôme Dubail, and Jesper Lykke Jacobsen. Inhomogeneous Gaussian free field inside the interacting arctic curve. *J. Stat. Mech. Theory Exp.*, (1):013102, 31, 2019.
[14] William Jockusch, James Propp, and Peter Shor. Random Domino Tilings and the Arctic Circle Theorem. *arXiv Mathematics e-prints*, page math/9801068, Jan 1998.
[15] Richard Kenyon. Lectures on dimers. In *Statistical mechanics*, volume 16 of *IAS/Park City Math. Ser.*, pages 191–230. Amer. Math. Soc., Providence, RI, 2009.
[16] Richard Kenyon, Wai Yeung Lam, Sanjay Ramassamy, and Marianna Russkikh. Dimers and Circle patterns. *arXiv e-prints*, page arXiv:1810.05616, Oct 2018.
[17] James Propp. Generalized domino-shuffling. volume 303, pages 267–301. 2003. Tilings of the plane.
[18] David E. Speyer. Perfect matchings and the octahedron recurrence. *J. Algebraic Combin.*, 25(3):309–348, 2007.
[19] William P. Thurston. Conway's tiling groups. *Amer. Math. Monthly*, 97(8):757–773, 1990.

Holder of the ENS–MHI chair funded by MHI. Département de mathématiques et applications de l'ENS, Ecole normale supérieure PSL Research University, CNRS UMR 8553, Paris 5ème. On leave from St. Petersburg Department of Steklov Mathematical Institute RAS.

E-mail address: `dmitry.chelkak at ens.fr`

Université Paris-Saclay, CNRS, CEA, Institut de physique théorique, 91191 Gif-sur-Yvette, France

E-mail address: `sanjay.ramassamy at ipht.fr`